JOURNAL OF SOLID STATE CHEMISTRY 65, 178–189 (1986)

Preparation, Properties, and Crystal Structure of the Solid Electrolytes $Cu_2P_3I_2$ and $Ag_2P_3I_2$*

M. H. MÖLLER AND W. JEITSCHKO

Anorganisch-Chemisches Institut, Universität Münster, Corrensstrasse 36, D-4400 Münster, West Germany

Received December 4, 1985; in revised form February 24, 1986

The new compound $Cu_2P_3I_2$ is a diamagnetic semiconductor with a susceptibility of $\chi = -193 \times 10^{-6}$ cm³/mole and a band gap of $E_a = 0.72$ eV. Its crystal structure is monoclinic, space group $P2_1/c$, with the lattice constants $a = 15.343(2)$ Å, $b = 12.925(2)$ Å, $c = 15.260(2)$ Å, $\beta = 116.38(1)°$, and $Z = 16$ formula units per cell. Twinning wrongly suggests orthorhombic and tetragonal symmetry. The crystal structure was determined from single-crystal X-ray data and refined to a residual of $R = 0.068$ and 4330 independent structure factors and 197 variable parameters. The P atoms form tubes similar to those in the Hittorf modification of phosphorus. They are surrounded by Cu atoms on 15 equipoint positions with occupancies varying between 0.15(1) and 0.97(1). These in turn are surrounded by iodine atoms which are well localized and form one-dimensional infinite channels. The structural characteristics suggest high mobility of the Cu^+ ions. This was proven by an ion exchange reaction of the $Cu_2P_3I_2$ crystals in aqueous $AgNO_3$ solution, which forms the new isotypic compound $Ag_2P_3I_2$. Transference measurements in a cell $Ag/Ag_2P_3I_2/Ag$ show that the electrical conductivity is essentially due to the transport of Ag^+ ions. The Ag^+ conductivity of $Ag_2P_3I_2$ at 140°C was determined to $\sigma = 3.5 \times 10^{-3}\ \Omega^{-1}$ cm^{-1}. $Ag_2P_3I_2$ is diamagnetic with a susceptibility of $\chi = -227 \times 10^{-6}$ cm³/mole.

Introduction

Our investigations of the binary systems copper and silver with phosphorus resulted in the preparation and structural characterization of the compounds Ag_3P_{11} (*1*) and Cu_2P_7 (*2*). In samples with lower phosphorus contents we have also prepared crystals (*2*) of the previously reported compounds CuP_2 and AgP_2 (*3*). In Cu–P samples, where iodine was added to obtain better crystallized products, we had occasionally observed a new compound, $Cu_2P_3I_2$, on which we report here. The isotypic compound $Ag_2P_3I_2$ seems to be metastable. It could only be prepared by reaction of the $Cu_2P_3I_2$ crystals with aqueous solutions of $AgNO_3$. A preliminary account of this work has been given elsewhere (*4*).

Synthesis of $Cu_2P_3I_2$

Samples of $Cu_2P_3I_2$ were prepared by reaction of the elemental components in evacuated sealed silica tubes. Starting materials were copper powder (Ventron, 200 mesh, 5N+), red phosphorus ("ultrapure," Hoechst-Knapsack), and iodine ("reinst," Merck). Prior to the reactions the copper powder was reduced in a stream of hydrogen at about 280°C, and the silica tubes

* In memory of Wilhelm Klemm (1896–1985), professor of inorganic chemistry in Münster.

0022-4596/86 $3.00

were heated to reduce their water content. The iodine was added in thin-walled closed capillaries which ruptured upon heating. Samples which contained $Cu_2P_3I_2$ could be prepared with a wide variety of starting compositions including the atomic ratios Cu : P from 1 : 1 to 1 : 4, Cu : I from 1 : 1 to 1 : 2, and P : I from 8 : 1 to 1 : 1. The samples were annealed for 7 days at temperatures varying between 500 and 650°C with a temperature difference of about 50°C over the length (~7 cm) of the tubes. At these temperatures the tubes are filled with a reddish brown gas, probably PI_3 and P_2I_4 (5), which upon cooling condenses to a reddish yellow, solid substance which is sensitive to hydrolysis. The total amount of the sample was calculated to yield a pressure between 10 and 20 bar at the reaction temperature.

The best yields of $Cu_2P_3I_2$ were obtained with the starting ratios Cu : P : I = 2 : 8 : 1 and 1 : 4 : 1 at a reaction temperature of about 550°C. In addition to $Cu_2P_3I_2$ the reaction products consisted of CuP_2, the Hittorf modification of phosphorus, and CuI even in samples with a high phosphorus content. Thus it seems that the ternary compound is thermodynamically stable only under a phosphorus vapor pressure of some bar at the reaction temperature. Pillar-shaped crystals of $Cu_2P_3I_2$ with a length of up to 4 mm were obtained at the hot end of the tubes, together with a small amount of CuI. The other reaction products were collected at the cooler end of the tubes. In the middle of the tubes very thin fibers of $Cu_2P_3I_2$ were identified.

Characterization of $Cu_2P_3I_2$

Crystals of $Cu_2P_3I_2$ cleave very easily with cleavage planes parallel to the needle axis yielding very thin woolly fibers. Large (mm size) crystals are stable in air for several weeks without visible deterioration. They can be dissolved only in oxidizing acids. Thermogravimetry under nitrogen in an open system shows decomposition beginning at 280°C; the solid reaction products being CuI and CuP_2 (Guinier powder diagrams).

A chemical analysis of $Cu_2P_3I_2$ was made in a wavelength-dispersive X-ray fluorescence spectrometer using properly prepared standards for comparison. The crystals of $Cu_2P_3I_2$ were dissolved in aqua regia in a closed container to avoid the loss of iodine which occurs as an intermediate reaction product. The two independent determinations, which gave the atomic ratios Cu/P/I of 1.96/3/1.89 and 2.16/3/1.95, are in good agreement with the ideal composition.

Electrical conductivities were measured for a pressed pellet of $Cu_2P_3I_2$ squeezed between flat tungsten contacts. The voltage difference was determined at constant current with a compensator. Because of the uncertainties of the contacting areas of and within the pellets no specific resistivities were calculated. However, the temperature dependence of the resistivity indicated semiconducting behavior. The band gap as determined from the slope of the $\ln R$ vs $1/T$ plot at high temperatures (between 320 and 460 K) according to the relation $R = R_0 \exp(E_a/2kT)$ is $E_a = 0.72$ eV.

Magnetic measurements of selected crystals, carried out with a Faraday balance, showed $Cu_2P_3I_2$ to be diamagnetic. The magnetic susceptibility is $\chi = -193 \times 10^{-6}$ cm^3/mole.

The Guinier powder diagrams of $Cu_2P_3I_2$ were indexed on the basis of the monoclinic cell obtained from the single-crystal study. This was facilitated by comparing the pattern with a theoretical diagram calculated (6) from the refined structure (Table I). The agreement between calculated and observed intensities is not perfect because of preferred orientation of the fibrous crystals. The following lattice constants were obtained by a least-squares calculation of 73 diffraction lines using α-quartz ($a = 4.9130$

TABLE I

GUINIER POWDER PATTERN OF $Cu_2P_3I_2$[a]

hkl'	hk l	Q_c	Q_o	I_c	I_o	hkl'	hk l	Q_c	Q_o	I_c	I_o
220	11-1	119	118	234	vw	833	04 3	1439		13	
202	00 2	214	213	28	vvw	206	40 2	1439	1441	44	m
400	20-2	237	236	295	w		31 3	1444		18	
	02 0	239	-	120			20 4	1446		13	
222	21 0	272	272	12	vvw	804	24 2	1573	1573	39	vw
013	10 2	362	360	26	vvw	824	61-2	1612	1610	42	vvw
213	21 1	420	419	25	vw	1002	60-4	1627	-	26	-
422	11-3	452	452	28	vvw	824	34 1	1630	-	116	s
251	31-2	467	-	39	-		21-6	1630	-	56	
233	31 0	536	537	27	vw		14 3	1634	1633	141	
	01 3	541	541	48	vw	862	53-3	1634	-	26	
620	31-3	592	592	1000	s	1002	15 1	1650	-	47	-
	13-1	598	598	569	w	844	62-2	1792	-	10	vvw
631	13-2	711	714	42	vvw		44 0	1805	1804	18	
433	32 0	716	-	32	-		22-6	1810	-	11	
053	10-4	720	720	29	vvw	1042	62-4	1866	-	20	
224	31 1	732	731	24	vw		42-6	1878	1878	13	vvw
640	32-3	772	773	122	w		35-1	1884	-	10	
404	40 0	847	846	61	w	1051	35-2	1903	-	14	vw
	00 4	856	-	26		880	44-4	1904	1904	84	
424	41 0	907	-	314	vs	475	12-6	1935	1935	23	vvw
	32 1	911	-	495		626	61 0	1966	1964	26	vw
	12 3	916	912	612		1033	05 3	1978	1976	26	vw
	01 4	916	-	374		266	43 2	1978	-	11	
651	33-2	945	-	33	m	1060	53-5	2017	2017	61	vw
800	40-4	946	948	388			35-3	2029	2027	62	vw
	04 0	958	958	426	m	864	63-2	2091		31	-
453	12-4	959	-	26	-		23-6	2109	2110	63	vw
015	30 2	974	974	55	m	1200	60-6	2129	-	29	-
471	42-3	1000	-	43	-	1025	71-3	2142	2141	74	vw
811	04 1	1011	-	119	vw		31-7	2165	-	38	-
820	14-1	1017	1019	49		1220	61-6	2189	-	44	-
215	21 3	1037	1036	52	w	891	44-5	2196	-	47	-
660	33-3	1071	1071	652	m	295	21-7	2231	2230	33	vvw
035	10 4	1098	1100	108	w	1071	35-4	2261	2260	33	vvw
235	41 1	1150	1156	107	w	1044	72-3	2321	2320	181	w
822	31-5	1165	-	39	-		45 0	2343	2346	330	s
840	42-4	1186	1187	48	vvw		32-7	2344	-	241	
291	51-4	1293	1293	28	vvw		05 4	2353	-	338	
813	14 2	1319	1318	27	vvw	1240	62-6	2369	-	44	-
842	52-3	1335	-	36	-	495	72-2	2385	-	48	-
	32-5	1344	-	29	vw	008	40 4	2460	2458	354	s
842	34-1	1346	1343	73		893	34-6	2509	-	26	-
	14-3	1350	-	29		884	64-2	2510	-	42	-
851	34-2	1364	-	25	-	1242	72-5	2515	2519	27	w
644	52-1	1380	1380	290	s	028	41 4	2520	-	20	
	43 0	1386	-	240		228	51 3	2574	2574	83	w
	12-5	1394	1393	270	s		31 5	2584	2582	62	w
	03 4	1395	-	250		846	14 5	2585	-	10	
						1035	45 1	2586	-	12	

[a] All observed lines and all lines with calculated intensities $I_c > 30$ are listed up to $Q = 2500$. The Q values are defined by $Q = 10^4/d^2$ Å^{-2}. The diagram was recorded with Cu$K\alpha_1$ radiation. The hkl values correspond to the true monoclinic cell, the values $h'k'l'$ to the pseudotetragonal cell.

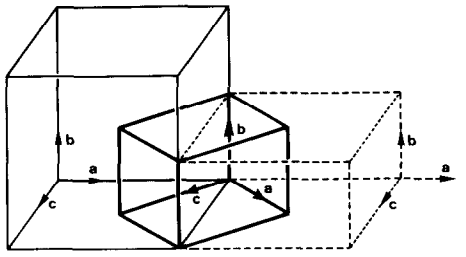

FIG. 1. Relation of the true monoclinic cell (thick lines) and the corresponding *B*-centered pseudo-orthorhombic cell (broken lines) to the pseudo-tetragonal cell of $Cu_2P_3I_2$. The pseudo-tetragonal cell of a twinned crystal (on the left) can be rationalized by the superposition of two orthorhombic cells, which differ in their orientation by a rotation of 90° around their common *c* axis.

Å, c = 5.4046 Å) as standard: a = 15.343(2) Å, b = 12.925(2) Å, c = 15.260(2) Å, β = 116.38(1)°, V = 2711 Å^3.

We have occasionally observed impurity lines in the powder diagrams which were caused by crystals of another ternary phase of the Cu–P–I system. Energy dispersive X-ray fluorescence analyses in a scanning electron microscope showed that these crystals have a higher phosphorus content than $Cu_2P_3I_2$. This phase was never observed as a major product in the samples.

Crystal Structure of $Cu_2P_3I_2$

Single crystals of $Cu_2P_3I_2$ were investigated in Buerger and Weissenberg cameras with Mo$K\alpha$ and Cu$K\alpha$ radiation. Their true symmetry is monoclinic with the lattice constants of the primitive cell as given in the previous section. In this conventional setting the needle axis corresponds to the [101] axis. The extinction conditions ($h0l$ observed only with $l = 2n$, $0k0$ only with $k = 2n$) lead to the unique space group $P2_1/c - C_{2h}^5$.

The strong reflections wrongly suggest orthorhombic symmetry. This pseudo-orthorhombic cell is *B* centered with the lattice constants a = 26.006 Å, b = 12.925 Å, c = 16.131 Å, $\alpha = \gamma = 90°$, β = 89.65°. They were obtained from the monoclinic cell by the transformation matrix 10-1/010/101. In this setting the needle axis of the crystals corresponds to the pseudo-orthorhombic *c* axis.

Some twinned crystals showed almost perfect tetragonal symmetry with the lattice constants a = 25.928 Å (the arithmetic mean of 26.006 and 2 × 12.925) and c = 16.131 Å. The diffraction patterns with the tetragonal symmetry, however, can be completely rationalized by the superposition of two reciprocal lattices. In the pseudo-orthorhombic setting the two lattices can be brought to coincide by a rotation of 90° around their common *c* axis. The relations of the monoclinic, pseudo-orthorhombic and pseudo-tetragonal cells are shown in Fig. 1. In addition to these "90° twins" we have also observed "180° twins." Their reciprocal lattices coincide if the lattice of one twin domain is rotated by 180° around the common pseudo-orthorhombic *c* axis of the twin domains.

The diffraction data for the structure determination of $Cu_2P_3I_2$ were recorded from a single crystal of dimensions 0.025 × 0.05 × 0.15 mm^3 with a four-circle diffractometer using Mo$K\alpha$ radiation, a graphite monochromator, a scintillation counter, and a pulse-height discriminator. The optimal scan rates of the θ–2θ scans were determined by fast prescans. Background counts were determined at both ends of each scan. A total of 17,719 reflections was recorded within one quadrant of reciprocal space up to 2θ = 80°. An empirical absorption correction (linear absorption coefficient μ = 160 cm^{-1}) was made from six azimuthal scans. The ratio of the maximum to the minimum transmission was 1.30. After averaging of equivalent reflections 9389 structure factors remained with $I_0 > \sigma(I_0)$. To improve the computer economy only those 4330 structure factors with $I_0 > 7\sigma(I_0)$ were used for the structure determination.

TABLE II

POSITIONAL AND THERMAL PARAMETERS OF $Cu_2P_3I_2$[a]

Atom	Occupancy	x	y	z	B
Cu(1)	0.97(1)	0.0997(2)	0.0328(3)	0.9038(2)	1.99(6)
Cu(2)	0.88(1)	0.0587(3)	0.2393(3)	0.4181(3)	2.03(7)
Cu(3)	0.85(1)	0.7690(3)	0.2364(3)	0.4527(3)	1.90(6)
Cu(4)	0.83(1)	0.8343(3)	0.2579(3)	0.1601(3)	1.91(7)
Cu(5)	0.65(1)	0.3250(4)	0.2073(5)	0.3779(4)	2.14(9)
Cu(6)	0.64(1)	0.7355(4)	0.9320(5)	0.5027(4)	2.17(10)
Cu(7)	0.61(1)	0.3538(4)	0.4301(5)	0.6192(4)	1.89(9)
Cu(8)	0.54(1)	0.5221(4)	0.8402(5)	0.2471(4)	1.70(9)
Cu(9)	0.39(1)	0.8765(6)	0.4508(7)	0.1418(6)	1.73(14)
Cu(10)	0.38(1)	0.5830(7)	0.2661(8)	0.4306(7)	2.16(16)
Cu(11)	0.37(1)	0.5488(7)	0.2386(9)	0.2260(7)	2.33(17)
Cu(12)	0.23(1)	0.3706(11)	0.1590(14)	0.1107(11)	2.29(27)
Cu(13)	0.21(1)	0.2458(12)	0.3395(16)	0.0166(12)	2.56(31)
Cu(14)	0.20(1)	0.5016(11)	0.4440(13)	0.2329(11)	1.47(25)
Cu(15)	0.15(1)	0.1106(15)	0.2116(19)	0.1662(16)	1.89(36)
P(1)	1	0.9757(4)	0.1075(5)	0.4453(4)	1.06(9)
P(2)	1	0.7802(4)	0.1278(5)	0.2172(4)	0.92(8)
P(3)	1	0.8157(4)	0.1186(5)	0.3733(4)	0.94(8)
P(4)	1	0.9921(4)	0.0522(5)	0.5915(4)	0.98(8)
P(5)	1	0.6251(4)	0.1177(5)	0.1846(4)	1.06(9)
P(6)	1	0.6792(4)	0.8788(5)	0.1356(4)	1.04(8)
P(7)	1	0.6268(5)	0.9532(6)	0.2326(5)	1.49(10)
P(8)	1	0.8175(4)	0.9662(5)	0.1844(4)	0.94(8)
P(9)	1	0.1349(4)	0.3772(5)	0.1788(4)	0.91(8)
P(10)	1	0.7701(4)	0.5440(5)	0.8752(4)	1.42(10)
P(11)	1	0.5876(4)	0.9463(5)	0.9908(4)	1.03(9)
P(12)	1	0.4433(4)	0.6093(5)	0.4761(4)	1.09(9)
I(1)	1	0.6917(1)	0.1240(1)	0.5447(1)	1.71(3)
I(2)	1	0.4423(1)	0.3511(1)	0.7979(1)	1.94(3)
I(3)	1	0.1825(1)	0.1442(1)	0.0622(1)	1.95(3)
I(4)	1	0.4348(1)	0.1591(1)	0.5633(1)	1.79(3)
I(5)	1	0.1502(1)	0.1433(1)	0.3319(1)	1.80(3)
I(6)	1	0.6640(1)	0.1233(1)	0.8345(1)	1.88(3)
I(7)	1	0.9276(1)	0.1674(1)	0.0747(1)	1.48(3)
I(8)	1	0.9280(1)	0.1220(1)	0.8145(1)	1.67(3)

Atom	U_{11}	U_{22}	U_{33}	U_{12}	U_{13}	U_{23}
I(1)	194(6)	176(7)	263(6)	11(6)	86(4)	−15(6)
I(2)	296(7)	247(8)	206(5)	82(6)	122(4)	68(6)
I(3)	286(7)	240(8)	175(6)	86(6)	67(5)	−26(6)
I(4)	237(6)	261(8)	158(5)	−60(6)	67(4)	32(6)
I(5)	283(6)	237(8)	156(5)	−41(6)	90(4)	28(6)
I(6)	193(6)	180(7)	328(7)	−21(6)	102(5)	3(7)
I(7)	196(5)	182(7)	205(5)	27(6)	108(4)	54(6)
I(8)	250(6)	168(6)	178(6)	43(6)	60(4)	−17(6)

[a] All atoms are in position 4*e* of space group $P2_1/c$. The standard deviations in the positions of the least significant digits are given in parentheses. The lower part of the table lists anisotropic thermal parameters $U(\times 10^4)$ of the iodine atoms defined by $\exp[-2\pi^2(h^2a^{*2}U_{11} + \cdots + hka^*b^*2U_{12} + \cdots)]$. The last row in the upper part of the table lists isotropic thermal parameters $B(A^2)$ of the Cu and P atoms and equivalent isotropic thermal parameters of the iodine atoms.

A partial solution of the structure was obtained by direct methods (*7*). Structural chemical considerations and subsequent difference Fourier syntheses led to the remaining atomic positions. Full-matrix least-squares refinements with atomic scattering factors (*8*), corrected for anomalous dispersion (*9*), resulted in unusually large thermal parameters for the Cu positions, some of which were also too close to each other to be fully occupied. In subsequent least-squares cycles the occupancy parameters of the Cu atoms were allowed to vary and additional Cu positions with low occupancies were added. Unit weights were used and a parameter accounting for isotropic secondary extinction was also refined.

In the final least-squares cycles, occupancy parameters and isotropic thermal parameters of the Cu atoms, which were refined simultaneously, converged to physically reasonable values (Table II). The iodine atoms were refined with ellipsoidal, the P atoms with isotropic thermal parameters. The composition $Cu_{1.97}P_3I_2$ thus obtained is in excellent agreement with the ideal composition of $Cu_2P_3I_2$ and the composition obtained by the quantitative X-ray fluorescence analysis. A final difference Fourier synthesis showed as highest peak an electron density of 5.4 e/Å^3 in a position too close to other atomic positions to be really occupied. The final conventional *R* value is 0.068 for 4330 structure factors and 197 variable parameters. A listing of observed and calculated structure factors is obtainable from the authors (*10*). Refinements where all atoms had isotropic and anisotropic thermal parameters, respectively, resulted in residuals of $R = 0.088$ (157 variables) and $R = 0.062$ (332 variables). In both cases the resulting composition was $Cu_{1.98}P_3I_2$.

Preparation and Ionic Conductivity of $Ag_2P_3I_2$

The structural characteristics of $Cu_2P_3I_2$ indicate high mobility for Cu^+ ions, which we wanted to prove. For this purpose we treated the crystals of $Cu_2P_3I_2$ with an aque-

ous solution of $AgNO_3$ (10 wt%). The crystals react immediately according to the equation

$$Cu_2P_3I_2 + 4Ag^+ = Ag_2P_3I_2 + 2Ag + 2Cu^{2+}$$

as can be seen by the formation of the blue complex $[Cu(OH_2)_4]^{2+}$. The silver is deposited mainly at the front faces of the elongated crystals (Fig. 2). The reaction is completed after about 15 min, as can be seen by the energy-dispersive analysis in a scanning electron microscope, and also by weight analysis (the spongy silver deposit dissolves faster in moderately diluted HNO_3 than the crystals of $Ag_2P_3I_2$).

The powder diffraction pattern of $Ag_2P_3I_2$ shows great similarity to that of $Cu_2P_3I_2$. The isotypy was proven by an intensity calculation (*6*). The lattice constants of $Ag_2P_3I_2$, refined by a least-squares treatment of the data, are $a = 15.81(3)$ Å, $b = 13.51(2)$ Å, $c = 15.93(4)$ Å, $\beta = 118.2(1)°$, $V = 2998$ Å^3. The increase of the cell volume from 2711 Å^3 for $Cu_2P_3I_2$ to 2998 Å^3 for the silver compound is the reason for the cracking of the crystals (Fig. 2).

We have not obtained $Ag_2P_3I_2$ by solid-state reactions in ways similar to those described above for $Cu_2P_3I_2$. Thus $Ag_2P_3I_2$ seems to be thermodynamically metastable. The preparation of this compound by ion exchange of $Cu_2P_3I_2$ with aqueous solutions of $AgNO_3$ yields products contaminated with elemental silver. Although silver dissolves faster in nitric acid than $Ag_2P_3I_2$, at least some solid AgI contaminates the thus formed reaction product.

Single-phase $Ag_2P_3I_2$, however, can be obtained by reaction of $Cu_2P_3I_2$ with an aqueous solution of $AgNO_3$ in the presence of an excess of KCN. Although the complex $[Ag(CN)_2]^-$ does not react as fast as Ag^+ ions with the $Cu_2P_3I_2$ crystals, no solid contamination product (Ag, CuI, or AgI) is formed and the reaction seems to proceed according to the equation

$$Cu_2P_3I_2 + 2[Ag(CN)_2]^- + 4CN^- = Ag_2P_3I_2 + 2[Cu(CN)_4]^{3-}.$$

The energy-dispersive analysis of the solid product in a scanning electron microscope showed no Cu impurities (detectability limit less than 1 at.% Cu).

$Ag_2P_3I_2$ is a gray fibrous material which smears upon grinding and is stable in air. Magnetic measurements with a Faraday balance at room temperature show $Ag_2P_3I_2$ to be diamagnetic with a susceptibility of $\chi = -227 \times 10^{-6}$ cm^3/mole.

To measure the electrical conductivity we have placed coldpressed pellets of $Ag_2P_3I_2$ between silver contacts. At room temperature the sum of both the specific electronic and the specific ionic conductivity is $\alpha = 6 \times 10^{-5}\ \Omega^{-1}\ cm^{-1}$. It increases linearly in a $\ln \sigma$ vs $1/T$ plot to about $\sigma = 8 \times 10^{-5}\ \Omega^{-1}\ cm^{-1}$ at 100°C. After that the conductivity increases much faster to reach a value of $\sigma = 3.5 \times 10^{-3}\ \Omega^{-1}\ cm^{-1}$ at 140°C. At this temperature the conductivity is essentially ionic as was proven in an independent transference experiment. An electric charge of 4.2 C (corresponding to 4.69 mg Ag) was transferred through a pellet of $Ag_2P_3I_2$ at 130°C. The weight loss of 4.62 mg at the silver anode shows that 99% of the current was transported by Ag^+ ions.

Discussion

The crystal structure of $Cu_2P_3I_2$ (and $Ag_2P_3I_2$) has a pronounced one-dimensional character. Tubes of condensed four- and five-membered rings of phosphorus atoms extend along the [101] direction (Figs. 3 and 4). Similar—although not identical—tubes of P atoms are known to occur in the Hittorf modification of elemental phorphorus (*12*), in $HgPbP_{14}$ (*13*), TlP_5 (*14*), CsP_{11} (*15*), KP_{15} (*16*), and BaP_{10} (*17*). In $Cu_2P_3I_2$ these tubes are surrounded by Cu atoms and these in turn are enveloped by iodine atoms. The projection of these parallel tubes

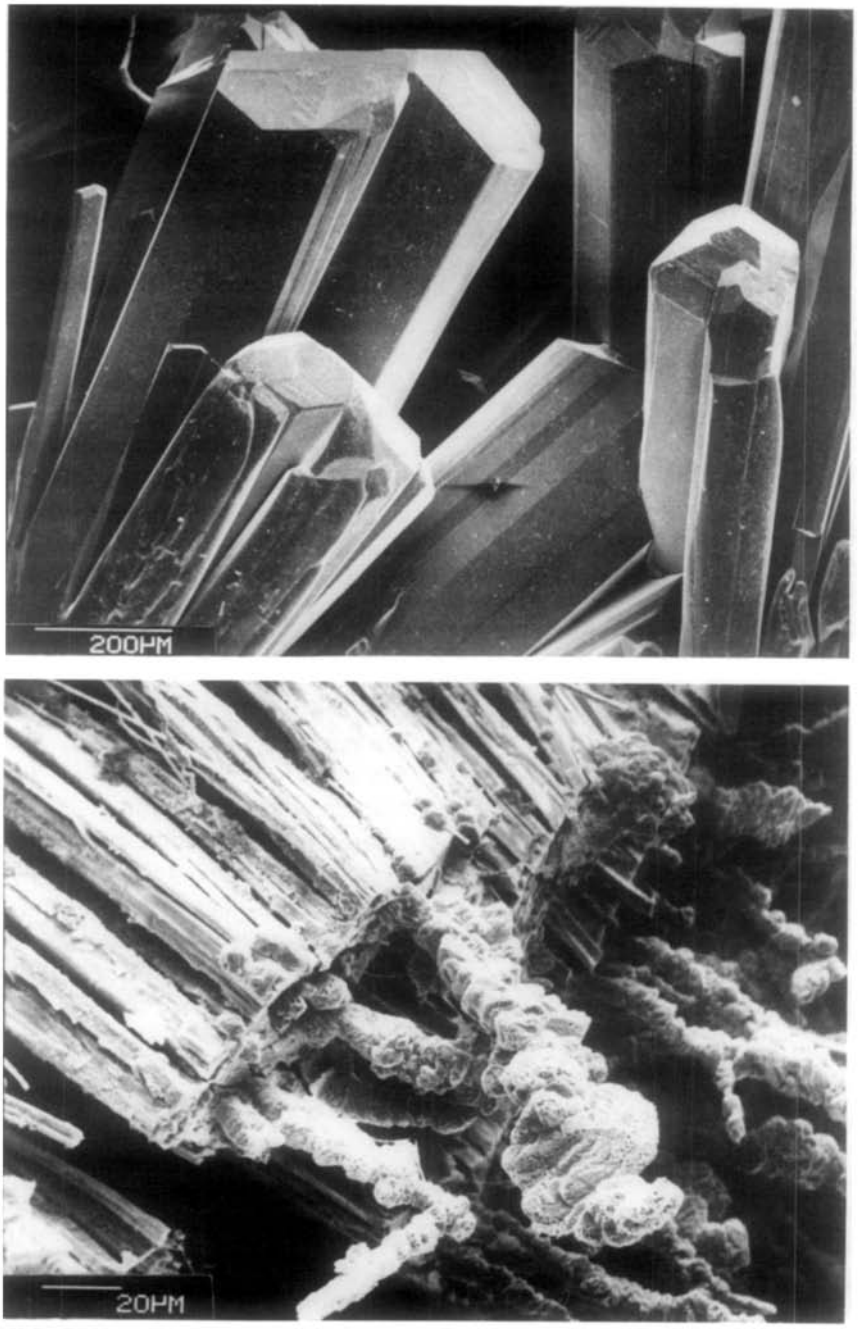

FIG. 2. Scanning electron micrographs of $Cu_2P_3I_2$ and $Ag_2P_3I_2$ crystals. In the upper part of the figure the end-faces of several needle-like crystals of $Cu_2P_3I_2$ are shown. In the lower micrograph at larger magnification the end-face of a former $Cu_2P_3I_2$ crystal is shown after reaction with a solution of $AgNO_3$. The crystal is split forming a large number of thin fibres of $Ag_2P_3I_2$. Spongy protrusions of elemental silver extend from the end-face of the former $Cu_2P_3I_2$ crystal diagonally to the lower right corner.

FIG. 3. A cutout of the tube-like chains of phosphorus atoms in the structure of $Cu_2P_3I_2$. One translation period of the chain consists of 24 P atoms arranged in two P_8 units—with a structure like the molecular compound As_4S_4 (*11*)—which are bridged by squares of P atoms in two different orientations.

along the tube axes results in a square mesh (Fig. 5). The pseudo-orthorhombic and pseudo-tetragonal twins observed for $Cu_2P_3I_2$ can be rationalized by considering, that the mismatch at the domain walls is caused essentially only by the rotation of the tubes, which in near-neighbor environments involves only the reorientation of a few Cu–I bonds.

The P–P bonds cover the range between 2.194 and 2.306 Å (Table III) with an average of 2.228 Å, slightly larger than the average P–P bond lengths of 2.199 Å in CuP_2 and 2.201 Å in Cu_2P_7 (*2*). Every P atom has three P atoms and one or two Cu positions as neighbors; none of the Cu positions, however, is fully occupied. In counting two valence electrons for each P–P interaction, the P atoms obtain oxidation number zero. There are no short P–I interactions. Since there are no short I–I interactions either, the oxidation number of the iodine atoms is −1 and the ideal formula is $Cu_2^{+1}P_3^0I_2^{-1}$.

There are 32 Cu atoms in the unit cell distributed over 60 atomic positions with occupancies ranging from 97 ± 1% for Cu(1) down to 15 ± 1% for Cu (*15*). Some Cu positions are so close to each other, that they cannot be occupied at the same time (Table III). All Cu positions are tetrahedrally coordinated to one P and three iodine positions all of which are fully occupied. The Cu–P bonds vary between 2.17 and 2.354 Å. The average bond length of 2.251 Å is close to the average Cu–P distance of 2.269 Å in Cu_4SnP_{10} (*18*), but slightly shorter than the corresponding distance (2.317 Å) in Cu_2P_7.

The iodine atoms have only Cu atoms as near neighbors. Four to seven such positions occur for each iodine atom at distances between 2.436 and 2.90 Å. However, when the occupancies of all neighboring Cu positions are considered,

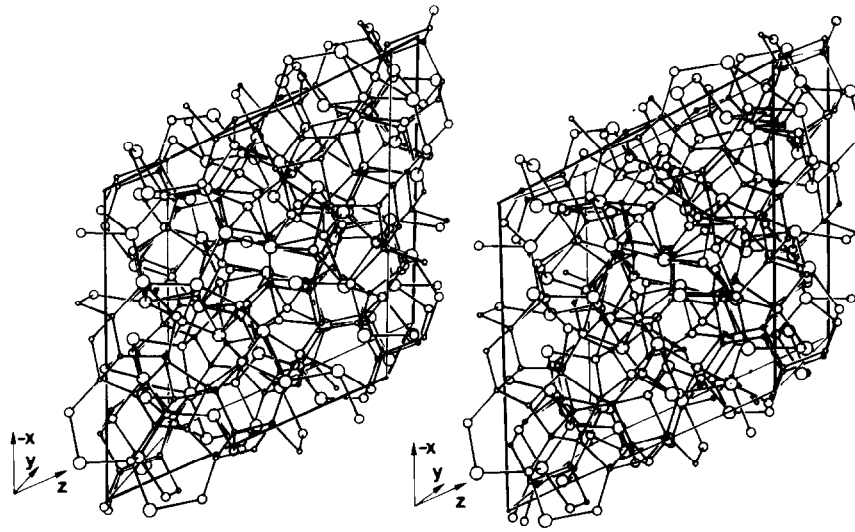

FIG. 4. Stereoplot of the $Cu_2P_3I_2$ structure. Small, medium, and large spheres correspond to phosphorus, copper, and iodine atoms, respectively.

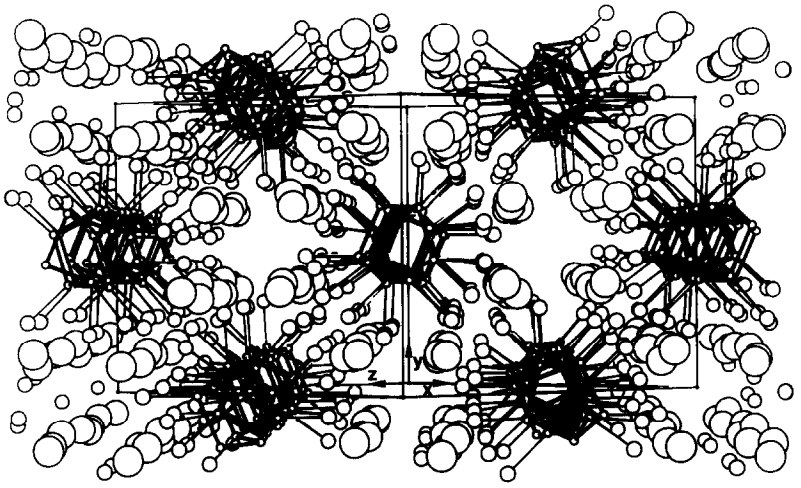

FIG. 5. Projection of the $Cu_2P_3I_2$ structure approximately along the [101] direction, the needle axis of the crystals. The dark tubes consisting of phosphorus atoms and open channels formed by the large iodine atoms are discernible. Medium-size circles are copper atoms.

the number of Cu neighbors varies only between 2.80 for I(7) and 3.09 for I(1).

In spite of the disorder of the copper atoms the compound is electronically saturated, as is demonstrated by the semiconductivity and the diamagnetism. The band gap of 0.72 eV is similar to the gap of 0.84 eV for Cu_2P_7.[1] The experimentally obtained diamagnetism of $\chi = -193 \times 10^{-6}$ cm^3/mole for $Cu_2P_3I_2$ and $\chi = -227 \times 10^{-6}$ cm^3/mole for $Ag_2P_3I_2$ may be compared with the calculated values of -206×10^{-6} cm^3/mole and -230×10^{-6} cm^3/mole, respectively.

For these calculations we have used the increments ($\chi \times 10^{-6}$ cm^3/mole) of -12 for Cu^+, -24 for Ag^+, -52 for I^-, and the Pascal increment of -26 for P^0 (*19, 20*). Thus the absolute calculated values are slightly too high and the difference between the values for the Cu and Ag compound is greater for the experimental than for the calculated values. It is interesting to consider these results together with the diamagnetism ($\chi \times 10^{-6}$ cm^3/mole) of -63 and -80 found for CuI and AgI (*20*). These compounds show the same difference per metal atom as our experimental values for $Cu_2P_3I_2$ and $Ag_2P_3I_2$. If we subtract the susceptibilities in the way $Cu_2P_3I_2 - Cu_2I_2$ and $Ag_2P_3I_2 - Ag_2I_2$ we obtain in both cases the same value of -67 for "P_3," e.g., an increment of -22.3×10^{-6} cm^3/mole for P^0. This increment for P^0, however, is not well defined since (because of the partial occupancy of the Cu positions) the P atoms in addition to their three P neighbors have either a Cu atom or a lone pair as fourth "ligand."

The structure of $Cu_2P_3I_2$ shows all characteristics of a solid electrolyte (*21–24*): partial occupancies for neighboring Cu positions which allow independent hopping from one site to the other, large thermal amplitudes of the Cu atoms indicating their loosely bound nature, and diffusion paths which extend throughout the structure. The importance of high polarizabilities of both the mobile species and the host lattice was also pointed out before (*25, 26*). The latter is the reason for the large number of solid electrolytes in various combinations of Cu^+ and Ag^+ with S^{2-}, Se^{2-}, Te^{2-}, and I^-.

[1] In the original publication (*2*) the activation energy was computed from E_a/kT; here we compare the values obtained from the expression $E_a/2kT$.

TABLE III

INTERATOMIC DISTANCES (Å) IN $Cu_2P_3I_2$[a]

Cu(1)–P(8)	2.224(5)	Cu(9)–P(4)	2.223(6)	P(1)–Cu(2)	2.272(6)	I(1)–Cu(10)	2.570(9)
I(3)	2.608(4)	I(8)	2.571(8)	P(3)	2.204(6)	Cu(4)	2.606(4)
I(8)	2.634(3)	I(5)	2.582(9)	P(4)	2.248(8)	Cu(3)	2.640(4)
I(7)	2.665(4)	I(1)	2.727(6)	P(4)	2.251(8)	Cu(6)	2.722(6)
Cu(2)–P(1)	2.272(6)	Cu(4)	2.621(10)	P(2)–Cu(4)	2.219(7)	Cu(9)	2.727(6)
I(5)	2.623(3)	Cu(6)	2.721(9)	P(3)	2.198(7)	I(2)–Cu(12)	2.568(15)
I(8)	2.630(4)	Cu(10)–P(12)	2.302(11)	P(5)	2.208(5)	Cu(11)	2.609(8)
I(3)	2.646(4)	I(1)	2.570(10)	P(8)	2.279(8)	Cu(7)	2.652(6)
Cu(13)	2.776(14)	I(2)	2.678(9)	P(3)–Cu(3)	2.252(6)	Cu(10)	2.678(9)
Cu(3)–P(3)	2.252(6)	I(6)	2.712(8)	P(2)	2.198(7)	Cu(8)	2.687(7)
I(6)	2.560(4)	Cu(8)	2.643(11)	P(1)	2.204(6)	Cu(5)	2.693(4)
I(7)	2.628(4)	Cu(3)	2.748(6)	P(10)	2.219(9)	Cu(14)	2.887(15)
I(1)	2.640(4)	Cu(11)	2.948(13)	P(4)–Cu(9)	2.223(6)	I(3)–Cu(15)	2.46(2)
Cu(10)	2.748(6)	Cu(11)–P(5)	2.206(10)	P(9)	2.194(6)	Cu(7)	2.561(4)
Cu(4)	2.865(5)	I(6)	2.539(10)	P(1)	2.248(8)	Cu(1)	2.608(4)
Cu(4)–P(2)	2.219(7)	I(2)	2.609(8)	P(1)	2.251(8)	Cu(2)	2.646(4)
I(7)	2.602(3)	I(4)	2.667(10)	P(5)–Cu(11)	2.206(10)	Cu(12)	2.649(10)
I(1)	2.606(4)	Cu(8)	(1.86(1))	P(12)	2.200(8)	Cu(13)	2.90(2)
I(8)	2.649(4)	Cu(12)	2.712(15)	P(2)	2.208(5)	I(4)–Cu(6)	2.625(4)
Cu(9)	2.621(10)	Cu(14)	2.76(2)	P(7)	2.244(9)	Cu(5)	2.645(5)
Cu(3)	2.865(5)	Cu(10)	2.948(13)	P(6)–Cu(5)	2.224(9)	Cu(13)	2.661(11)
Cu(5)–P(6)	2.224(9)	Cu(12)–P(11)	2.354(15)	P(7)	2.196(7)	Cu(8)	2.666(6)
I(5)	2.588(4)	I(2)	2.568(15)	P(11)	2.204(8)	Cu(11)	2.667(10)
I(4)	2.645(5)	I(3)	2.649(10)	P(8)	2.220(6)	Cu(14)	2.677(15)
I(2)	2.693(4)	I(4)	2.77(2)	P(7)–Cu(8)	2.254(7)	Cu(12)	2.77(2)
Cu(13)	2.934(15)	Cu(7)	(1.20(2))	Cu(14)	2.257(10)	I(5)–Cu(15)	2.49(2)
Cu(6)	2.988(7)	Cu(11)	2.712(15)	P(6)	2.196(7)	Cu(6)	2.541(6)
Cu(6)–P(10)	2.253(7)	Cu(13)	2.96(2)	P(5)	2.244(9)	Cu(13)	2.54(2)
I(5)	2.541(6)	Cu(13)–P(10)	2.32(2)	P(10)	2.306(8)	Cu(9)	2.582(9)
I(4)	2.625(4)	I(5)	2.54(2)	P(8)–Cu(1)	2.224(5)	Cu(5)	2.588(4)
I(1)	2.722(6)	I(4)	2.661(11)	P(9)	2.205(8)	Cu(2)	2.623(3)
Cu(13)	(1.29(2))	I(3)	2.90(2)	P(6)	2.220(6)	I(6)–Cu(14)	2.436(12)
Cu(9)	2.721(9)	Cu(6)	(1.29(2))	P(2)	2.279(8)	Cu(11)	2.539(10)
Cu(5)	2.988(7)	Cu(2)	2.776(14)	P(9)–Cu(15)	2.17(2)	Cu(3)	2.560(4)
Cu(7)–P(11)	2.238(6)	Cu(5)	2.934(15)	P(4)	2.194(6)	Cu(8)	2.600(4)
I(3)	2.561(4)	Cu(12)	2.96(2)	P(8)	2.205(8)	Cu(7)	2.643(6)
I(6)	2.643(6)	Cu(14)–P(7)	2.257(10)	P(10)	2.217(7)	Cu(10)	2.712(8)
I(2)	2.652(6)	I(6)	2.436(12)	P(10)–Cu(6)	2.253(7)	I(7)–Cu(15)	2.58(2)
Cu(12)	(1.20(2))	I(4)	2.677(15)	Cu(13)	2.32(2)	Cu(4)	2.602(3)
Cu(14)	2.87(2)	I(2)	2.89(2)	P(9)	2.217(7)	Cu(3)	2.628(4)
Cu(8)–P(7)	2.254(7)	Cu(8)	(1.46(2))	P(3)	2.219(9)	Cu(1)	2.665(4)
I(6)	2.600(4)	Cu(11)	2.76(2)	P(7)	2.306(8)	I(8)–Cu(9)	2.571(8)
I(4)	2.666(6)	Cu(7)	2.87(2)	P(11)–Cu(7)	2.238(6)	Cu(2)	2.630(4)
I(2)	2.687(7)	Cu(15)–P(9)	2.17(2)	Cu(12)	2.354(15)	Cu(1)	2.634(3)
Cu(14)	(1.46(2))	I(3)	2.46(2)	P(6)	2.204(8)	Cu(4)	2.649(4)
Cu(11)	(1.86(1))	I(5)	2.49(2)	P(12)	2.242(5)		
Cu(10)	2.643(11)	I(7)	2.58(2)	P(12)	2.265(9)		
				P(12)–Cu(10)	2.302(11)		
				P(5)	2.200(8)		
				P(11)	2.242(5)		
				P(11)	2.265(9)		

[a] None of the copper positions is fully occupied. For occupancy factors see Table II. For the Cu and P atoms all distances shorter than 3 Å are listed. The iodine atoms have no near neighbors at distances less than 3.7 Å except for the Cu atoms listed. The shortest I–P and I–I distances are 3.717 and 3.906 Å.

The main diffusion paths which allow the high mobility of the cations in $Cu_2P_3I_2$ and $Ag_2P_3I_2$ are not clear. No high electron densities were found in the open one-dimensional channels formed by the iodine atoms. Nevertheless it could be that a relatively small number of metal ions moves fast in these channels. On the other hand, the large number of neighboring partially occupied Cu positions suggests hop-

ping between these partially occupied sites. The PI_3 coordination tetrahedra of these sites are linked by common faces and edges in continuous cross-linked chains with short Cu–Cu distances of about 3 Å or less. They extend throughout the structure, not only along the needle axis (the [101] direction) of the crystals. The experimental evidence, however, that the elemental silver, produced by the redox reaction of $Cu_2P_3I_2$ with aqueous solution of $AgNO_3$, is deposited mainly at the end-faces of the needle-like crystals, suggests high mobility mainly along the needle axis.

The Ag^+ conductivity measurements of $Ag_2P_3I_2$ do not show a sharp discontinuity within the measured range from room temperature to 160°C. Thus in spite of the relatively large increase of the ionic conductivity within this temperature range, a phase transition between an ordered nonconducting and a disordered conducting structure, as it is known for AgI (*27*) and several other solid electrolytes (*28*), does not occur. Such a phase transition is also difficult to imagine in view of the complex structure with 15 different crystallographic metal positions of broadly varying occupancies. The experimentally determined Ag^+ conductivity for $Ag_2P_3I_2$ of 3.5×10^{-3} $\Omega^{-1}cm^{-1}$ at 140°C is not spectacular in view of the high conductivity of 1.3 $\Omega^{-1}cm^{-1}$ at 150°C already determined by Tubandt and Lorenz for AgI (*29*). The solid electrolyte with the highest ionic conductivity at room temperature, $RbAg_4I_5$ (*28, 30, 31*), has a conductivity of 2.5×10^{-1} Ω^{-1} cm^{-1}. Nevertheless, the complexity of the structure of $Cu_2P_3I_2$ and $Ag_2P_3I_2$ with the broad range of occupancies for the Cu (and as yet undetermined for the Ag) positions is unusual.

Acknowledgments

We want to thank Dr. U. Flörke for magnetic measurements, Mrs. Ch. Zweig for work on the scanning electron microscope, Dr. E. Lechtenberg and Prof. Dr. D. Klockow for support in X-ray fluorescence spectrometry, Dr. H.-D. Wiemhöfer and Prof. Dr. H. Rickert (all at that time at Universität Dortmund) for advice concerning the transference measurements. We are also indebted to Dr. G. Höfer (Heraeus Quarzschmelze) for a gift of silica tubes and to the Hoechst-Knapsack AG for a sample of ultrapure red phosphorus. This work was supported by the Deutsche Forschungsgemeinschaft and the Fonds der Chemischen Industrie.

References

1. M. H. MÖLLER AND W. JEITSCHKO, *Inorg. Chem.* **20,** 828 (1981).
2. M. H. MÖLLER AND W. JEITSCHKO, *Z. Anorg. Allg. Chem.* **491,** 225 (1982).
3. O. OLOFSSON, *Acta Chem. Scand.* **19,** 229 (1965).
4. M. H. MÖLLER AND W. JEITSCHKO, Eighth Europ. Crystallogr. Meeting, Liège (1983), Abstracts, p. 209.
5. H. SCHÄFER AND M. TRENKEL, *Z. Anorg. Allg. Chem.* **391,** 11 (1972).
6. K. YVON, W. JEITSCHKO, AND E. PARTHÉ, *J. Appl. Crystallogr.* **10,** 73 (1977).
7. P. MAIN, Computer Program MULTAN 11/82. Physics Dept. University of York, England.
8. D. T. CROMER AND J. B. MANN, *Acta Crystallogr. Sect. A* **24,** 321 (1968).
9. D. T. CROMER AND D. LIBERMAN, *J. Chem. Phys.* **53,** 1891 (1970).
10. M. H. MÖLLER, Dissertation, Universtät Dortmund, FRG, 1983.
11. D. J. E. MULLEN AND W. NOWACKI, *Z. Kristallogr.* **136,** 48 (1972).
12. A. THURN AND H. KREBS, *Acta Crystallogr. Sect. B* **25,** 125 (1969).
13. H. KREBS AND T. LUDWIG, *Z. Anorg. Allg. Chem.* **294,** 257 (1958).
14. O. OLOFSSON AND J. GULLMAN, *Acta Chem. Scand.* **25,** 1327 (1971).
15. H. G. v. SCHNERING, *in* "Homoat. Rings, Chains Macromol., Main-Group Elem." (A. L. Rheingold, Ed.), p. 317, Elsevier, Amsterdam, 1977.
16. H. G. v. SCHNERING AND H. SCHMIDT, *Angew. Chem.* **79,** 323 (1967), *Int. Ed.* **6,** 356 (1967).
17. H. G. v. SCHNERING AND G. MENGE, *Z. Anorg. Allg. Chem.* **491,** 286 (1982).
18. W. HÖNLE AND H. G. v. SCHNERING, *Z. Kristallogr.* **153,** 339 (1980).
19. W. KLEMM, "Magnetochemie," Akad. Verlagsges., Leipzig, 1936.
20. LANDOLT-BÖRNSTEIN, New Series II/2, Springer, Berlin, 1966.

21. S. GELLER, *in* "Fast Ion Transport in Solids," Conf. Proc. (W. van Gool, Ed.), p. 609, North-Holland, Amsterdam, 1973.
22. W. L. ROTH AND O. MULLER, "The Study, Selection, and Preparation of Solid-State Cationic Conductors," NASA Report CR-134610, 1974.
23. W. JEITSCHKO, T. A. BITHER, AND P. E. BIERSTEDT, *Acta Crystallogr. Sect. B* **33,** 2767 (1977).
24. P. MCGEEHIN AND A. HOOPER, *J. Mater. Sci.* **12,** 1 (1977).
25. H. WIEDERSICH AND S. GELLER, *in* "The Chemistry of Extended Defects in Non-Metallic Solids," Conf. Proc. (L.-R. Eyring and M. O'Keeffe, Ed.), p. 629, North-Holland, Amsterdam, 1970.
26. R. D. ARMSTRONG, R. S. BULMER, AND T. DICKINSON, *J. Solid State Chem.* **8,** 219 (1973).
27. K. FUNKE, *Prog. Solid State Chem.* **11,** 345 (1976).
28. M. O'KEEFFE AND B. G. HYDE, *Philos. Mag.* **33,** 219 (1976).
29. C. TUBANDT AND E. LORENZ, *Z. Phys. Chem.* **87,** 513 (1914).
30. S. GELLER, *Acc. Chem. Res.* **11,** 87 (1978).
31. H. RICKERT, "Electrochemistry of Solids," Springer, Berlin, 1982.